Evidence for carrier-mediated magnetism in Mn-doped ZnO thin films

Devajyoti Mukherjee, Tara Dhakal, Hariharan Srikanth, Pritish Mukherjee, and Sarath Witanachchi*
Department of Physics, University of South Florida, Tampa, Florida 33620, USA
(Received 15 January 2010; revised manuscript received 30 March 2010; published 6 May 2010)

In this paper, we demonstrate through experiments and analysis that the most probable mechanism for the observed ferromagnetism in 2% Mn-doped ZnO thin films is a combination of intrinsic and carrier-mediated interaction of the magnetic moments. While no impurity-phase contributions were detected, a strong correlation between effective carrier densities and ferromagnetism was established. Magnetism in amorphous films with high defect densities were described by a bound magnetic polaron model whereas that in highly conducting films was consistent with a Ruderman-Kittel-Kasuya-Yosida exchange mechanism.

DOI: 10.1103/PhysRevB.81.205202 PACS number(s): 75.50.Pp, 71.38.−k, 81.15.Fg

Almost a decade has passed since the theoretical predictions by Dietl *et al.*[1] about room-temperature (RT) ferromagnetism (FM) in Mn-doped ZnO (ZMO) and the potential applications as spintronic devices that had started an extensive research effort in transition metal doped ZnO. The high solubility of 3*d* metals in ZnO has added another interesting functionality to this multifunctional material that exhibits useful optical, electrical, and piezoelectric properties. However diverse experimental results ranging from paramagnetism,[2] spin glass,[3] anti-FM (AFM),[4] low-temperature FM,[5] to even RT FM[6–8] have been reported over the years. Sharma *et al.*[6] who were the first to report the RT FM had shown that Mn when doped nominally in ZnO was in Mn^{2+} valence state and the FM was carrier induced. In contrast Kundaliya *et al.*[7] later suggested that the FM was due to an oxygen-vacancy-stabilized $Mn_{2-x}Zn_xO_{3-\delta}$ phase rather than carrier-induced interaction among separate Mn atoms in ZnO matrix. Subsequently, García *et al.*[8] showed that the RT FM in the ZMO was associated with the coexistence of Mn^{3+} and Mn^{4+} via a double-exchange mechanism. Such conflicting arguments produced no consensus on the origins of FM in ZMO systems. A fundamental understanding of the mechanism of magnetism in these materials is essential in order to achieve desired properties for use in device applications. Further experimental reports on effects of growth conditions such as substrate temperature (T_s) and oxygen pressure on the magnetic properties of ZMO films grown by pulsed laser deposition suggested that higher saturation magnetization (M_s) was observed in the conducting films grown at a T_s of 500–600 °C and a low background pressure of O_2.[9,10] All these varied reports only emphasized the fact that the observed FM was very sensitive to sample preparation, crystalline quality, residual defects, and resulting carrier concentrations. In 2005, Coey *et al.*[11] proposed a defect mediated bound magnetic polaron (BMP) model to explain the FM in ZMO. In recent papers such defect mediated FM was experimentally observed.[10,12] More recently, Calderon and Sarma[13] proposed a model based on two complementary magnetic mechanisms—the BMP percolation at low temperatures in insulating samples and the indirect RKKY exchange mechanism in more conducting samples at temperatures where substantial thermally activated carriers were present in the impurity band.[14,15] However, there have been no direct observations that have validated this model. In this paper we present experimental and theoretical evidence suggesting that the dual FM model[13] may finally resolve some of the controversies associated with origins of FM in ZMO systems.

A series of Mn-doped ZnO films were grown at different substrate temperatures from a $Zn_{0.98}Mn_{0.02}O$ ceramic target on 10×5 mm^2 c-cut sapphire substrates by conventional pulsed laser deposition using a KrF excimer laser (248 nm, 10 Hz, and 40 ns) operating at 154 mJ/pulse giving a fluence of 2 J/cm^2 at the target surface which was 6 cm away from the substrate. The stoichiometric target was fabricated by conventional solid state reaction techniques described in Refs. 6 and 9. The average atomic percent Mn in the target was determined by energy dispersive x-ray analysis to be $2.0\pm0.4\%$. The background O_2 pressure during deposition was kept constant at 10 mT to fix one of the parameters that could contribute to intrinsic oxygen vacancies and related charged carriers. The film thicknesses were in the range of 400–460 nm.

In order to rule out the presence of other phases of Mn in our thin films a careful x-ray diffraction analysis was conducted. Figure 1 shows the θ-2θ XRD scans of films deposited at T_s of RT, 200, 400, and 600 °C. Films grown at these temperatures are labeled as ZMO(RT), ZMO(200), ZMO(400), and ZMO(600), respectively. The films were highly textured with no observed peaks from secondary phase formation within the resolution limits of XRD. The log scale for intensity was used to exaggerate the low intensity peaks so that if secondary phases are present, they can be identified easily. The improved crystallinity with higher T_s was indicated by the increase in peak intensities (Fig. 1) and decrease in the full width at half maximum (FWHM) of rocking curves about (002) plane of ZnO (Table I). Scanning electron microscopy imaging and AFM surface analysis further confirmed the improved crystallinity, hexagonal faceting, grain coalescing, and increased surface roughness with higher T_s. All the above observations were consistent with previous reports.[5,9]

The resistivity and carrier concentrations measured at 300 K by the van der Pauw configuration are summarized in Table I. All the measured films showed *n*-type conduction with an overall increase in resistivity and decrease in mobility in the doped films as compared to undoped ZnO film. The film ZMO(RT) was highly insulating with very low density of free carriers. This could also be associated with the poor crystalline nature of the film which made the system strongly disordered.

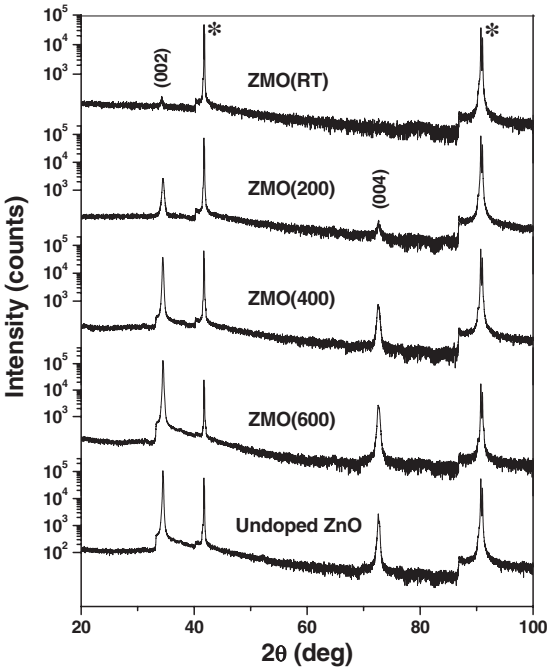

FIG. 1. XRD patterns of $(Zn_{0.98}Mn_{0.02})O$ films on sapphire substrates grown at room temperature, 200, 400, and 600 °C with a background oxygen pressure of 10 mT named as ZMO(RT), ZMO(200), ZMO(400), and ZMO(600), respectively. The sapphire substrate peaks have been denoted by *.

The magnetic properties of all the films were measured using a commercial physical property measurement system (PPMS) from Quantum Design fitted with a vibrating-sample magnetometer option. All the samples were handled very carefully to avoid any trace magnetic contamination. They were always handled with gloves using nonmagnetic tweezers and kept in closed dry containers. The substrates were cleaned by standard acetone-methanol ultrasonication. The samples were loaded in nonmagnetic capsules using nonmagnetic tape in the PPMS probe. The substrates were checked for magnetic contamination before deposition. Figure 2 shows the *M-H* hysteresis loops measured at 300 and 10 K for ZMO films deposited at different temperatures. The background diamagnetic contribution due to the sapphire substrates has been corrected consistently in all the presented curves. An increase in the 300 K saturation magnetization (M_s) from 1.08 ± 0.02 to 1.67 ± 0.02 emu/cm^3 and coercivity (H_c) from ~120 to ~250 Oe were observed as the T_s was increased from RT to 600 °C. At 10 K, H_c increased from ~110 to ~180 Oe and M_s increased from 2.17 ± 0.03 to 3.1 ± 0.1 emu/cm^3 from the film ZMO(RT) to ZMO(600). The increase in H_c from ZMO(RT) to ZMO(600) most likely is related to the increase in grain size with higher T_s.[9] The H_c and M_s for films ZMO(200) and ZMO(400) also followed the same trend. Further, to confirm the role of Mn doping in enhancing the FM of ZMO films, *M* vs *H* loops

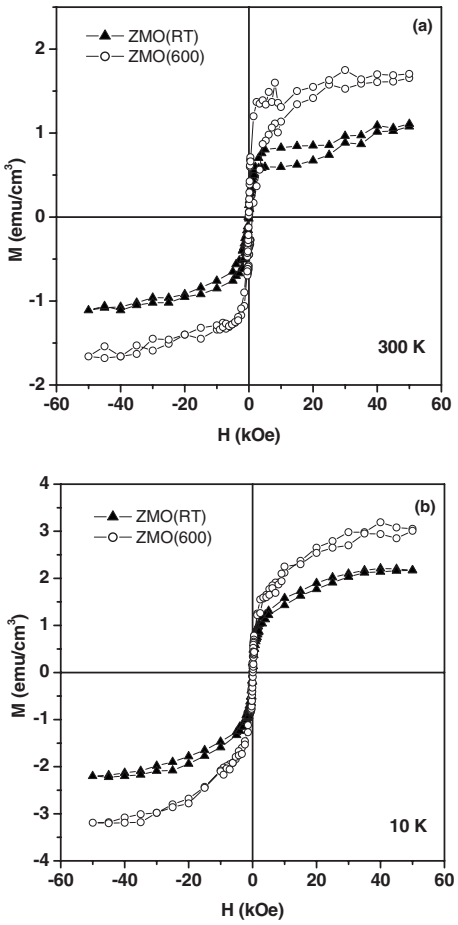

FIG. 2. *M* vs *H* loops measured at (a) 300 K and (b) 10 K for $(Zn_{0.98}Mn_{0.02})O$ films deposited at RT and 600 °C with a constant background oxygen gas pressure of 10 mT named as ZMO(RT) and ZMO(600), respectively. The magnetic field has been applied parallel to the film plane.

TABLE I. FWHM of rocking curves about (002) plane of ZnO, average crystallite size using Scherrer formula, resistivity (ρ), and carrier concentration (n_c) measured at room temperature for $(Zn_{0.98}Mn_{0.02})O$ films deposited at various growth temperatures with a constant background oxygen gas pressure of 10 mT.

Sample	Growth temperatures T_s (°C)	FWHM (deg) of rocking curve	Crystallite size D (nm)	ρ (Ω cm)	n_c (cm^{-3})
ZMO(RT)	RT	n.a.	41	1.36×10^4	7.78×10^{12}
ZMO(200)	200	2.307	54	9.69	2.89×10^{17}
ZMO(400)	400	1.399	54	8.33	3.88×10^{17}
ZMO(600)	600	0.417	56	0.46	2.51×10^{18}
UndopedZnO	600	0.404	50	0.02	1.04×10^{18}

were also measured for the film ZMO(600) and the undoped ZnO film both grown at T_s of 600 °C under the same conditions. The M_s for ZMO(600) was found to be four times higher than undoped ZnO film, both showing room temperature ferromagnetism as previously reported.[16] On the other hand there was no appreciable change in H_c and M_s for ZMO(600) from M vs H loops measured for magnetic fields applied parallel or perpendicular to film plane.[17] This absence of anisotropic ferromagnetism suggests a weak contribution from magnetic point defects which was very large for Co-doped ZnO thin films as reported by Venkatesan *et al.*[11,17]

We argue here that at 10 K, in the film ZMO(RT), which is highly insulating, it is the percolation of BMPs that give rise to the observed magnetism. In contrast, films deposited at 200, 400, and 600 °C, which are more conducting, it is the indirect RKKY mechanism which dominates the magnetic behavior.[13] Since both mechanisms depend on thermally generated carriers, the activation energies (ΔE) for ZMO(RT) and ZMO(600) were estimated by fitting the resistivity curves to the expression, $\rho=\rho_o \exp(\Delta E/k_BT)$. The value of ΔE for ZMO(RT) and ZMO(600) were ~6.4 and ~42.4 meV, respectively. The larger density of defects associated with the poor crystalline quality of ZMO(RT) contributed to a shallower donor level than in ZMO(600) due to Mn doping.

Over three decades back, Smith[18] had reported that the measured magnetization in dilute magnetic ZnMn or CuMn alloys was dominated by impurity-impurity interaction via the indirect RKKY potential. In a high magnetic field (H) such that $g\mu_B H \gg k_BT$ and n_iV_o the approach to saturation of the magnetization (M) follows the relation

$$M = g\mu_B S n_i[1 - 2(2S+1)n_iV_o/3g\mu_B H], \quad (1)$$

where n_i is the concentration of the active magnetic impurities (Mn^{2+}) interacting via RKKY, V_o is the strength of RKKY interaction, and $S=5/2$ is the spin of magnetic impurity.[6] However, in our case $g\mu_B H \sim k_BT$ but is $\gg n_iV_o$. From the slopes and intercepts of the linear fits of M vs $1/H$ data points at saturation measured at 10 K, for ZMO(200), ZMO(400) and ZMO(600), we calculated n_i and V_o using Eq. (1). Figure 3 shows the linear fits. The calculated values have been summarized in Table II. The intercepts and slopes increased slightly from ZMO(200) to ZMO(600). This showed that the number of magnetic impurities interacting via RKKY mechanism increased with higher T_s and better crystallinity. However the slope of the linear fit for ZMO(RT) was different than the others showing a smaller value for n_i. The calculated value of n_i for ZMO(600) was $n_i \sim 7.31\times10^{19}$ cm^{-3}. It was much lower than the magnetic impurity density for 2 at. % doping of Mn in ZnO which was 8.438×10^{20} cm^{-3}. In other words only ~8% of the total number of Mn^{2+} ions in the system were involved in RKKY mediated FM. From Fig. 2(b) for ZMO(600) the M_s was ~3.1 emu/cm^3 which corresponded to an average magnetic moment of $0.4\mu_B/Mn^{2+}$ assuming a uniform Mn ion distribution. This was again 8% of the theoretical value which was $5\mu_B/Mn^{2+}$ when all the Mn spins are aligned.[1,6] Thus only about 8% of the incorporated Mn atoms at substitutional Zn sites contributed to FM via RKKY mechanism.

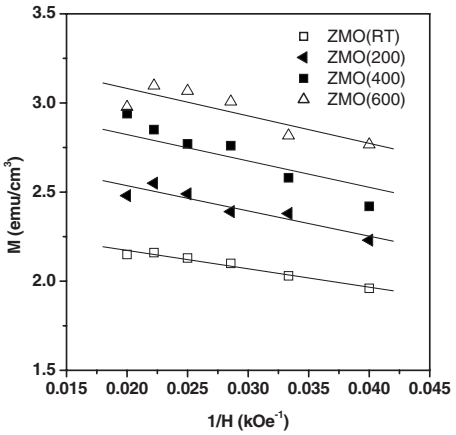

FIG. 3. Magnetization as a function of $1/H$ (kOe^{-1}) at 10 K for $(Zn_{0.98}Mn_{0.02})O$ films deposited at various growth temperatures with constant background oxygen pressure. The solid lines are the linear fits of M vs $1/H$ data points for films named ZMO(RT), ZMO(200), ZMO(400), and ZMO(600).

The remaining Mn atoms may have formed interstitial defect sites or accumulated at the grain boundaries. However, the contribution of interstitial Mn ion to FM via a defect mediated mechanisms such as BMP has been shown to be very small[11] and therefore does not account for the observed magnetism in our highly crystalline ZMO (600) films. Further, the carrier density (n_c) at 10 K for ZMO(600) estimated using $n_c(T)=n_{co}\exp(\Delta E/k_BT)$ for the measured values of n_c (300 K) and ΔE was $n_c \sim 2.01\times10^{16}$ cm^{-3}. Since $n_c \ll n_i$ or in other words the mean distance between the carriers was greater than that between the spins, RKKY interaction would give FM as predicted by Priour *et al.*[19] The average value of $V_o \approx (5.96+/-0.85)\times10^{-37}$ erg cm^3 was consistent with those observed by Smith.[18] Moreover, the average value of $n_iV_o \approx 0.02$ meV($<k_BT$), the spin-spin interaction energy for RKKY, was smaller than the thermal energy at 10 K (0.863 meV) ensuring the availability of enough carriers to mediate RKKY FM even at such low temperatures.

In order to explain the FM in ZMO(RT) we used a defect mediated model. In this BMP model, the electron confinement radius (a_B) was calculated using $a_B=\varepsilon(m_o/m_e^*)a$, where ε is the static dielectric constant, $m_e^*=0.28m_o$ is the electron effective mass, and $a=0.52$ Å is the Bohr radius.[16] First, the value of ε was computed from the capacitance measurements of the films using a Hewlett Packard 4192A High Frequency Impedance Analyzer at 1 MHz and 1 V rms oscillation voltage. The value of ε for ZMO(600) was 1.95 ± 0.36 but for ZMO(RT) the value was higher than the impedance limit of the instrument. Second, ε for ZMO(RT) and ZMO(600) were computed using the Brus equation[20,21] where the change in band gap was equated to the activation energy (ΔE) measured earlier and the crystal radius was calculated from Scherrer formula as in Table I. The ε values for ZMO(RT) and ZMO(600) were 11.3 and 2.06, respectively. The electron confinement radii for ZMO(RT) and ZMO(600) were ~20 Å and ~4 Å, respectively. The radius value for ZMO(RT) was larger owing to the shallower defect level ($\Delta E \sim 6.4$ meV).[16] The BMP model is valid only in the low carrier density regime where $n_ca_B^3 \ll 1$ and when $n_i \gg n_c$. This

TABLE II. Summary of RKKY parameters calculated using the linear fits in Fig. 3.

Sample	Intercept	Slope	n_i (10^{19} cm^{-3})	V_o (10^{-37} erg cm^3)	n_iV_o (meV)
ZMO(RT)	2.3741	10314	5.12	6.75	0.0216
ZMO(200)	2.8173	14166	6.08	6.58	0.0250
ZMO(400)	3.1209	14782	6.73	5.59	0.0235
ZMO(600)	3.3896	15399	7.31	4.94	0.0226

was true for both ZMO(RT) and ZMO(600). Following Calderon and Sarma's[13] work the temperature dependence of the radius of the polaron (R_P) was plotted using the equation

$$R_P(T) \equiv (a_B/2)\ln[sS|J|(a_0/a_B)^3/k_BT], \quad (2)$$

where $s=\frac{1}{2}$ the spin of carriers (electrons), $S=5/2$ the spin of magnetic dopant (Mn^{2+}), using $J\approx 1$ eV the local exchange coupling between carrier spin and the magnetic Mn moments[11,18] and $a_0^3=47.77$ Å^3 the unit-cell volume for ZnO. Figure 4 shows the curves for the ZMO(RT) and ZMO(600). For ZMO(RT), polarons only start forming at a temperature of $T_{initiation}\sim sS|J|(a_0/a_B)^3/k_B\sim 75$ K above which there are no polarons in the system. However in ZMO(600) polarons are always present even at room temperature. The size of the BMPs in ZMO(RT) increases drastically from ~0.7 Å at 70 K to ~20 Å at 10 K whereas for ZMO(600) the increase in size is gradual from ~7 Å at 300 K to ~13 Å at 10 K. The magnetic dopant spins at a distance $r<R_P$ tend to align with the localized carrier spin. The average separation between randomly oriented magnetic dopant spins was found to be ~10 Å, which is based on the relation $r=(1/n_i)^{1/3}$ where $n_i=8.438\times 10^{20}$ cm^{-3} for 2 at. % doping of Mn in ZnO. With lowering of temperature, polarons start overlapping with neighboring BMPs forming FM clusters which keep growing in size to form an infinite cluster (of the size of the system), i.e., when the BMP percolation occurred. The percolation radius (r_{perc}) for ZMO(RT) at 10 K is ~5 μm calculated from $r_{perc}\approx 0.86/n_c^{1/3}$ (Ref. 18), where n_c (10 K) was estimated using $n_c(T)=n_{co}\exp(\Delta E/k_BT)$ from $n_c(RT)$ and ΔE values measured earlier. The r_{perc} in ZMO(RT) was larger than the thickness of the film and implied long range FM at 10 K. The r_{perc} for ZMO(600) at 10 K was 0.03 μm which was much smaller than the film thickness to mediate large FM via BMP percolation throughout the sample. From Fig. 4 we also see that for ZMO(600), $R_p\approx r$, in the range 10–300 K. This implies that the BMPs are always overlapping with their spins aligned with the carriers. If there are substantial thermally activated carriers, the BMP scenario extrapolates to RKKY FM.

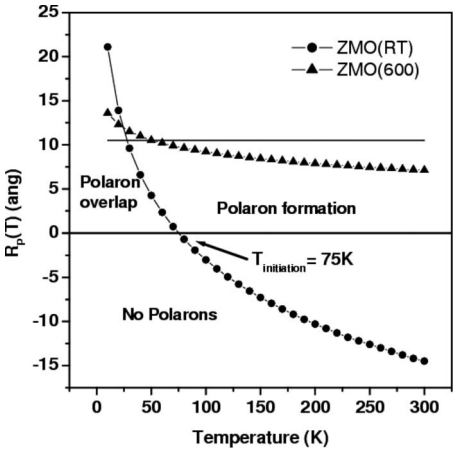

FIG. 4. Variation in the radius of polarons R_p in angstroms at different temperatures for ZMO(RT) and ZMO(600), $(Zn_{0.98}Mn_{0.02})O$ films deposited at RT and 600 °C, respectively.

In conclusion we have demonstrated that the observed FM in $Zn_{0.98}Mn_{0.02}O$ films shows characteristics of both intrinsic and carrier-mediated mechanisms. The experimental results show a strong correlation between effective carrier densities due to different growth conditions and the FM in our samples. The data are consistent with the dual ferromagnetic theoretical model proposed for dilute magnetic semiconductors (DMS). Although these results are encouraging for a fundamental understanding of the origins of the observed ferromagnetic phases in DMS, higher values of saturation magnetization at room temperature would be required for any potential device application.

This work was supported in part by the NSF (Grants No. DMI-0217939 and No. DMI-0078917) and by the Department of Defense (Grant No. W81XWH-07–1-0708). H.S. thanks support from the Department of Energy BES through Grant No. DE-FG02–07ER46438.

*Corresponding author; switanac@cas.usf.edu

[1] T. Dietl, H. Ohno, F. Matsukura, J. Cibert, and D. Ferrand, Science **287**, 1019 (2000).
[2] X. M. Cheng and C. L. Chien, J. Appl. Phys. **93**, 7876 (2003).
[3] T. Fukumura, Z. Jin, M. Kawasaki, T. Shono, T. Hasegawa, S. Koshihara, and H. Koinuma, Appl. Phys. Lett. **78**, 958 (2001).
[4] G. Lawes, A. S. Risbud, A. P. Ramirez, and R. Seshadri, Phys. Rev. B **71**, 045201 (2005).
[5] S. W. Jung, S. J. An, G. C. Yi, C. U. Jung, S. Lee, and S. Cho,

Appl. Phys. Lett. **80**, 4561 (2002).
[6] P. Sharma, A. Gupta, K. V. Rao, F. J. Owens, R. Sharma, R. Ahuja, J. M. Osorio Guillen, B. Johansson, and G. A. Gehring, Nature Mater. **2**, 673 (2003).
[7] D. C. Kundaliya, S. B. Ogale, S. E. Lofland, S. Dhar, C. J. Metting, S. R. Shinde, Z. Ma, B. Varughese, K. V. Ramanujachary, L. Salamanca-Riba, and T. Venkatesan, Nature Mater. **3**, 709 (2004).
[8] M. A. García, M. L. Ruiz-González, A. Quesada, J. L. Costa-Krämer, J. F. Fernández, S. J. Khatib, A. Wennberg, A. C. Caballero, M. S. Martín-González, M. Villegas, F. Briones, J. M. González-Calbet, and A. Hernando, Phys. Rev. Lett. **94**, 217206 (2005).
[9] A. K. Pradhan, K. Zhang, S. Mohanty, J. B. Dadson, D. Hunter, J. Zhang, D. J. Sellmyer, U. N. Roy, Y. Cui, A. Burger, S. Mathews, B. Joseph, B. R. Sekhar, and B. K. Roul, Appl. Phys. Lett. **86**, 152511 (2005).
[10] S. Ramachandran, J. Narajan, and J. T. Prater, Appl. Phys. Lett. **88**, 242503 (2006).
[11] J. M. D. Coey, M. Venkatesan, and C. B. Fitzgerald, Nature Mater. **4**, 173 (2005).
[12] Q. Xu, H. Schmidt, L. Hartmann, H. Hochmuth, M. Lorenz, A. Setzer, P. Esquinazi, C. Meinecke, and M. Grundmann, Appl. Phys. Lett. **91**, 092503 (2007).
[13] M. J. Calderon and S. Das Sarma, Ann. Phys. (N.Y.) **322**, 2618 (2007).
[14] X. Zuo, S.-D. Yoon, A. Yang, W.-H. Duan, C. Vittoria, and V. G. Harris, J. Appl. Phys. **105**, 07C508 (2009).
[15] Z. Yang, M. Biasini, W. P. Beyermann, M. B. Katz, O. K. Ezekoye, X. Q. Pan, Y. Pu, J. Shi, Z. Zuo, and J. L. Liu, J. Appl. Phys. **104**, 113712 (2008).
[16] N. H. Hong, J. Sakai, and V. Brize, J. Phys.: Condens. Matter **19**, 036219 (2007).
[17] M. Venkatesan, C. B. Fitzgerald, J. G. Lunney, and J. M. D. Coey, Phys. Rev. Lett. **93**, 177206 (2004).
[18] F. W. Smith, Phys. Rev. B **10**, 2980 (1974); **14**, 241 (1976).
[19] D. J. Priour, Jr., E. H. Hwang, and S. Das Sarma, Phys. Rev. Lett. **92**, 117201 (2004).
[20] L. Brus, J. Phys. Chem. **90**, 2555 (1986).
[21] C. K. Ghosh, K. K. Chattopadhyay, and M. K. Mitra, J. Appl. Phys. **101**, 124911 (2007).